

# Vacancy assisted arsenic diffusion and time dependent clustering effects in silicon

Benjamin P. Haley and Niels Grønbech-Jensen

*Department of Applied Science, University of California, Davis CA 95616*

(Dated: November 14, 2018)

## Abstract

We present results of kinetic lattice Monte Carlo (KLMC) simulations of substitutional arsenic diffusion in silicon mediated by lattice vacancies. Large systems are considered, with 1000 dopant atoms and long range *ab initio* interactions, to the 18th nearest lattice neighbor, and the diffusivity of each defect species over time is calculated. The concentration of vacancies is greater than equilibrium concentrations in order to simulate conditions shortly after ion implantation. A previously unreported time dependence in the applicability of the pair diffusion model, even at low temperatures, is demonstrated. Additionally, long range interactions are shown to be of critical importance in KLMC simulations; when shorter interaction ranges are considered only clusters composed entirely of vacancies form. An increase in arsenic diffusivity for arsenic concentrations up to  $10^{19} \text{ cm}^{-3}$  is observed, along with a decrease in arsenic diffusivity for higher arsenic concentrations, due to the formation of arsenic dominated clusters. Finally, the effect of vacancy concentration on diffusivity and clustering is studied, and increasing vacancy concentration is found to lead to a greater number of clusters, more defects per cluster, and a greater vacancy fraction within the clusters.

## I. INTRODUCTION

The diffusion of dopants, such as arsenic, in silicon has been studied extensively because of its importance in integrated circuit manufacturing. Native point defects, such as lattice vacancies, which may be created during implantation of the dopants, interact with other defects to facilitate diffusion of the implanted species. As circuit device sizes continue to shrink, approaching the scale of typical diffusion distances, a deeper understanding of this phenomenon is critical.

The effects of temperature on the diffusion process have been studied experimentally and theoretically. The experimentally measured diffusivity of arsenic is known to increase as temperature increases.<sup>1</sup> Several theoretical models have, as expected, demonstrated the same result due to greater thermal fluctuations at higher temperatures. A previous kinetic lattice Monte Carlo (KLMC) study<sup>2</sup> showed how defect capture radii depend on interaction range and temperature. Bunea and Dunham<sup>3</sup> used a KLMC model with one arsenic, one vacancy, and interactions ranging from the third to sixth nearest lattice neighbor site. They found an increase in arsenic diffusivity at higher temperatures, and quantified deviations from a pair diffusion model in terms of a correction factor introduced into Fick's first law<sup>4</sup>. As temperature increased, the value of the correction factor deviated more from the expected value of 1. They also demonstrated that deviations from pair diffusion increased with a longer interaction range. Pankratov *et al.*<sup>5</sup> also used a KLMC model with a single arsenic and vacancy and interactions extending from the third to 20th nearest neighbor to show that arsenic diffusivity increases with temperature. They demonstrated that a "ring mechanism", in which a vacancy moves along a hexagonal ring around an arsenic atom, contributes less to arsenic diffusion at higher temperatures and that this effect is more significant for longer interaction ranges. In section III A we present the results of similar KLMC calculations, with 1000 arsenic atoms and 100 vacancies and long range interactions. In section III B we study the effect of interaction range on diffusion and clustering.

The effect of arsenic concentration on diffusivity and cluster formation has been studied because of its relation to the electrical deactivation of arsenic at high doping levels. Fair and Weber<sup>6</sup> experimentally found maximum arsenic diffusivity with arsenic concentration of  $3 \times 10^{20} \text{ cm}^{-3}$  at 1000 °C. The diffusivity of arsenic decreased for concentrations above and below this level. Larsen *et al.*<sup>7</sup> found that arsenic diffusivity increased for arsenic

concentrations above  $2 \times 10^{20} \text{ cm}^{-3}$  at  $1050 \text{ }^\circ\text{C}$ . Solmi and Nobili<sup>8</sup> demonstrated an increase in arsenic diffusivity for concentrations up to  $3.5 \times 10^{20} \text{ cm}^{-3}$  and constant diffusivity for higher concentrations.

KLMC simulations have also given differing results. Dunham and Wu<sup>9</sup> found, using estimated third nearest neighbor interactions at  $1050 \text{ }^\circ\text{C}$ , an increase in arsenic diffusivity at high doping levels, in agreement with Larsen *et al.*<sup>7</sup>. Bunea and Dunham<sup>10</sup> used a similar KLMC model, with third nearest neighbor *ab initio* interactions at  $900 \text{ }^\circ\text{C}$ , and found enhancement over short simulation times, up to  $10^4$  time steps, but the enhancement diminished over longer simulation times. List and Ryssel<sup>11</sup> also performed KLMC simulations similar to those of Dunham and Wu<sup>9</sup> but found no diffusivity enhancement. All of these KLMC simulations used vacancy concentrations which depended on the temperature and the equilibrium vacancy concentration,  $C_V^0$ . Experiments<sup>12</sup> performed at  $1050 \text{ }^\circ\text{C}$  measured  $C_V^0 = 3 \times 10^{15} \text{ cm}^{-3}$ . The value most commonly used in KLMC simulations, included those cited above, was  $C_V^0 = 5 \times 10^{16} \text{ cm}^{-3}$ , which is still a dilute concentration but large enough to allow for reasonable system sizes in KLMC simulations.

Xie and Chen<sup>13</sup> summarized all these discrepancies, experimental and theoretical, and concluded that time dependent clustering effects were responsible. They performed *ab initio* calculations and showed that interactions to at least the ninth nearest neighbor were important and that a short term arsenic diffusivity enhancement would die out due to formation of clusters larger than arsenic-vacancy pairs. In section III C, we present our KLMC results, with long range (18th nearest neighbor) *ab initio* interactions, for several arsenic concentrations, and a constant arsenic:vacancy ratio. In this work, we assume a large vacancy concentration, which would be expected post-implantation. In section III D we vary the arsenic:vacancy ratio to determine what effect vacancy concentration has on diffusion and clustering.

## II. SIMULATION METHOD

### A. Kinetic Lattice Monte Carlo

We use a kinetic lattice Monte Carlo (KLMC) method to simulate atomic scale diffusion processes. This method visits defects on a silicon lattice, either randomly or in some pre-

determined order, and, if a move is allowed, attempts to move each defect, one at a time. Defects include substitutional dopants and native point defects, which include vacancies in this work. Possible movements include vacancies exchanging lattice sites with lattice atoms or defects. Although concerted exchange is a theoretical possibility<sup>14</sup>, we do not consider it in this work. Thus, a move is allowed if the defect in question is a vacancy, or if the defect in question is a dopant, and a randomly chosen neighboring site is occupied by a vacancy. If a move is attempted, the change in the system energy determines whether the move is accepted. If the move lowers energy, it is accepted. If the move does not lower energy, it is accepted, according to the Metropolis detailed balance algorithm, with probability  $e^{-\Delta E/2k_B T}$ , where  $k_B$  is Boltzmann’s constant,  $T$  is the system temperature, and  $\Delta E$  is the change in system energy as a result of the move. The system energy in each configuration is the sum of pair interactions between the defects. The values for the pair interactions at given separations on the lattice, out to 18 neighbors, were calculated with *ab initio* methods described in subsection B.

The time scale of a KLMC simulation is set by the hopping frequency,  $\nu_H$ , of the defects, which is determined by

$$\nu_H = \nu_0 e^{-E_b/k_B T} \quad (1)$$

where  $\nu_0$  is the attempt frequency,  $E_b$  is the height of the energy barrier for the move,  $k_B$  is Boltzmann’s constant, and  $T$  is the system temperature. In this work, for vacancies, we used  $\nu_0^V$  calculated with the expression

$$\nu_0 = \frac{8D_0}{a_0^2}, \quad (2)$$

and the values  $D_0^V = 1.18 \times 10^{-4}$  cm<sup>2</sup>/s, and  $E_b^V = 0.1$  eV, reported for low density vacancy diffusion by Tang *et al.*<sup>15</sup>, and a lattice constant of 5.43 Å. Since this value for  $E_b$  is less than the 0.2 eV used by Bunea and Dunham<sup>3,10</sup>, our vacancy hopping frequency is higher. For the attempt frequency of arsenic, we scaled the attempt frequency of vacancies

$$\nu_0^{As} = \sqrt{\frac{m_V}{m_{As}}} \nu_0^V \quad (3)$$

where  $m_V$  is the effective mass of a vacancy (or the mass of a silicon atom) and  $m_{As}$  is the mass of an arsenic atom. We used 0.58 eV as the energy barrier for arsenic–vacancy exchange, as reported by Pankratov *et al.*<sup>5</sup>.

After each KLMC step, which visits all defects in the system, the simulation time is incremented by the time step of the fastest allowed event, which in this work is the exchange of a vacancy with a Si lattice atom, set by  $\nu_H^V$ . For events with longer time steps, such as the exchange of a vacancy with an arsenic atom, an attempt is made at each time step if a randomly generated number between 0 and 1 is less than, for example,

$$\frac{\nu_H^{As}}{\nu_H^V}. \quad (4)$$

KLMC methods follow the position of each defect in the system over time. This allows the definition of a diffusion coefficient as

$$D(t_1, t_2) = \frac{\langle |r_i(t_2) - r_i(t_1)|^2 \rangle_i}{6 |t_2 - t_1|}, \quad (5)$$

which approaches the thermodynamic diffusion coefficient as  $|t_2 - t_1|$  approaches infinity. We use this definition in order to study diffusion during various time ranges.

## B. *Ab initio* Calculations

The pair interactions between vacancies<sup>16</sup> and between vacancies and arsenic<sup>2</sup> were calculated using the ultrasoft pseudopotential plane wave code VASP<sup>17</sup>, on a 216 atom supercell. The generalized gradient approximation (GGA) was used, along with a  $4^3$  Monkhorst-Pack<sup>18</sup>  $\mathbf{k}$ -point sampling and a kinetic energy cutoff of 208 eV. All vacancies were charge neutral. The arsenic-arsenic interactions were calculated using PEtot<sup>19</sup>, a norm conserving pseudopotential plane wave code, on a 64 atom supercell, using the local density approximation (LDA) and a  $2^3$  Monkhorst-Pack  $\mathbf{k}$ -point sampling and a kinetic energy cutoff of 218 eV. In each case, the initial configuration of atoms was allowed to relax and the final energy was recorded for all possible separations of each defect pair. The results are shown in Figure 1. In this work, separate defects were not permitted to simultaneously occupy the same lattice site.

## III. RESULTS

For the following sections, we began with a baseline system containing 1000 arsenic atoms and 100 vacancies on a silicon lattice measuring 84 unit cells on each side for an arsenic

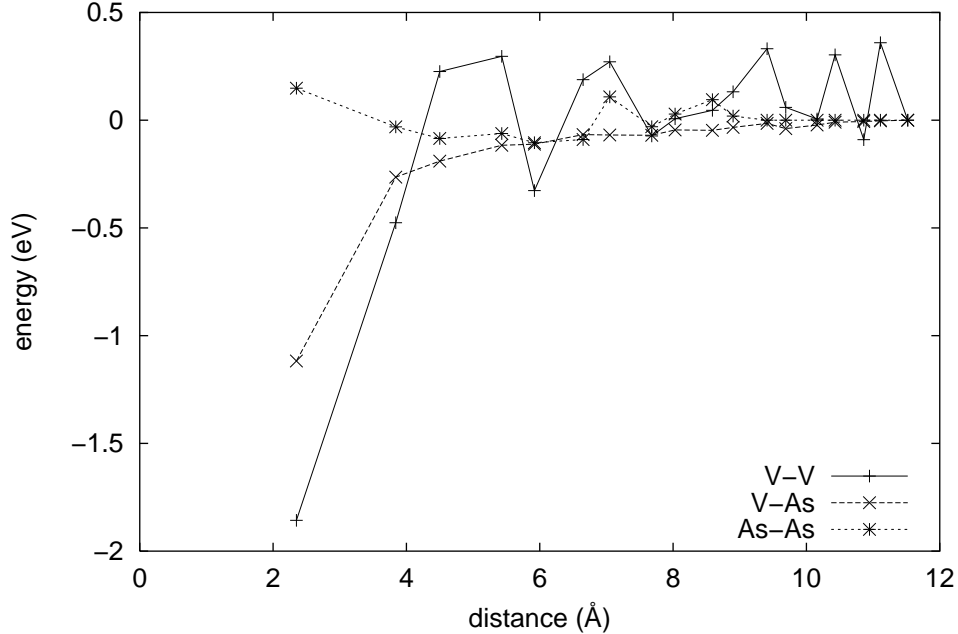


FIG. 1: Pair interaction energies for vacancies and arsenic.

concentration of  $10^{19} \text{ cm}^{-3}$ . Boundary conditions were periodic, and pair interactions to the 18th nearest neighbor were considered. The base system temperature was 900 K. In subsection A, we vary the temperature, while the interaction range varies in subsection B. In subsection C we consider various arsenic concentrations, and in subsection D we vary the arsenic:vacancy ratio. Each simulation presented is the mean of five identical simulations. We define a cluster as two or more defects, substitutional arsenic or vacancies, occupying a nearest neighbor position from at least one other member of the cluster.

### A. Temperature

In this section we vary the system temperature while holding the number of arsenic and vacancies, the system size, and the interaction range constant. Figure 2 shows the diffusivity, calculated using equation (5), of arsenic and vacancies as a function of time for temperatures ranging from 700 K to 1300 K. The quantity  $t_2$  in equation (5) represents the continuing system time, and  $t_1$  is reset to  $t_2$  when  $t_2 - t_1$  is twice as large as the previous time interval. We see that the vacancies diffuse freely at first, while the arsenic atoms are stationary. At all temperatures the free vacancy diffusivities match the theoretical values, which are shown on Figure 2 for times earlier than the first data point on the vacancy

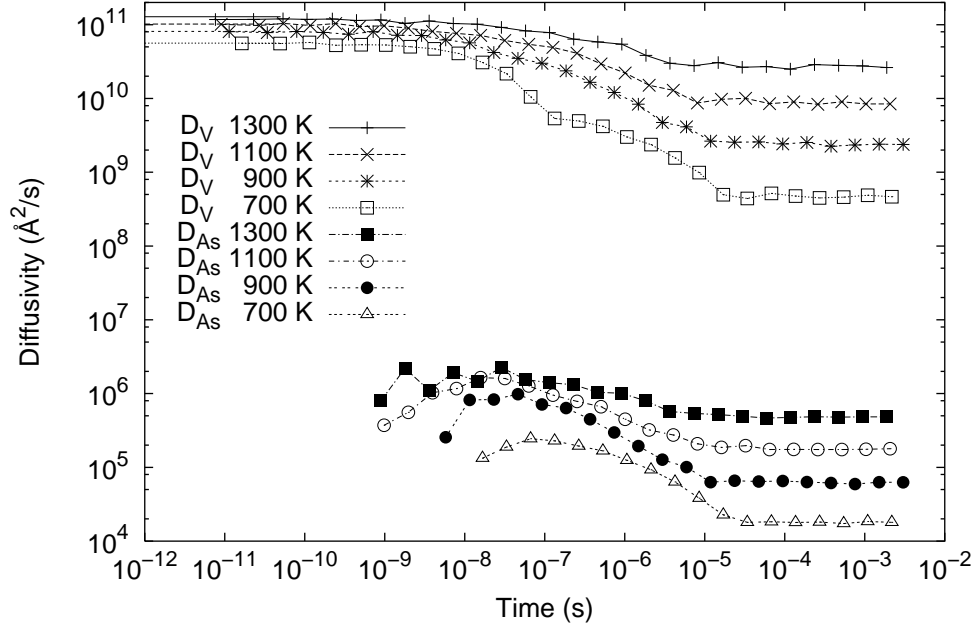


FIG. 2: Diffusivity of arsenic and vacancies over time for various temperatures, with arsenic concentration  $10^{19} \text{ cm}^{-3}$  and vacancy concentration  $10^{18} \text{ cm}^{-3}$  and 18 shell interactions.

diffusivity curves. As arsenic-vacancy pairs (AsV) form, the arsenic begins to diffuse. The diffusivity of both species is greater at higher temperatures, as expected, since the thermal fluctuations  $k_B T$  are larger relative to the migration energy of both AsV and free vacancies, and by  $10^{-5}$  seconds the transient effects disappear. In Figure 3, the fraction of the total number of defects which are free (not in a cluster) is shown over time for each species. At higher temperatures, fewer defects are in clusters. The same trends can be seen in Figure 4, which shows the number of clusters and the number of defects per cluster over time. More clusters form at lower temperatures and these are largely arsenic-vacancy pairs (AsV) for times up to approximately  $10^{-7}$  seconds. At that time the number of clusters peaks for lower temperatures, and the number of defects per cluster rises above two for all temperatures. At higher temperatures, fewer clusters form, but those that do form are slightly larger on average. Figure 5 shows that the vacancy fraction of defects in clusters increases over time for all temperatures considered. For lower temperatures, this implies that AsV begin to aggregate, as indicated in Figure 4a, and that some of the AsV dissociate, as in Figure 3a, with the vacancy attaching itself to another AsV. At higher temperatures the number of clusters is more stable over time, as in Figure 4a, which implies that mobile AsV attract free vacancies. In either case, a pair diffusion model is only valid for a short time, roughly  $10^{-7}$

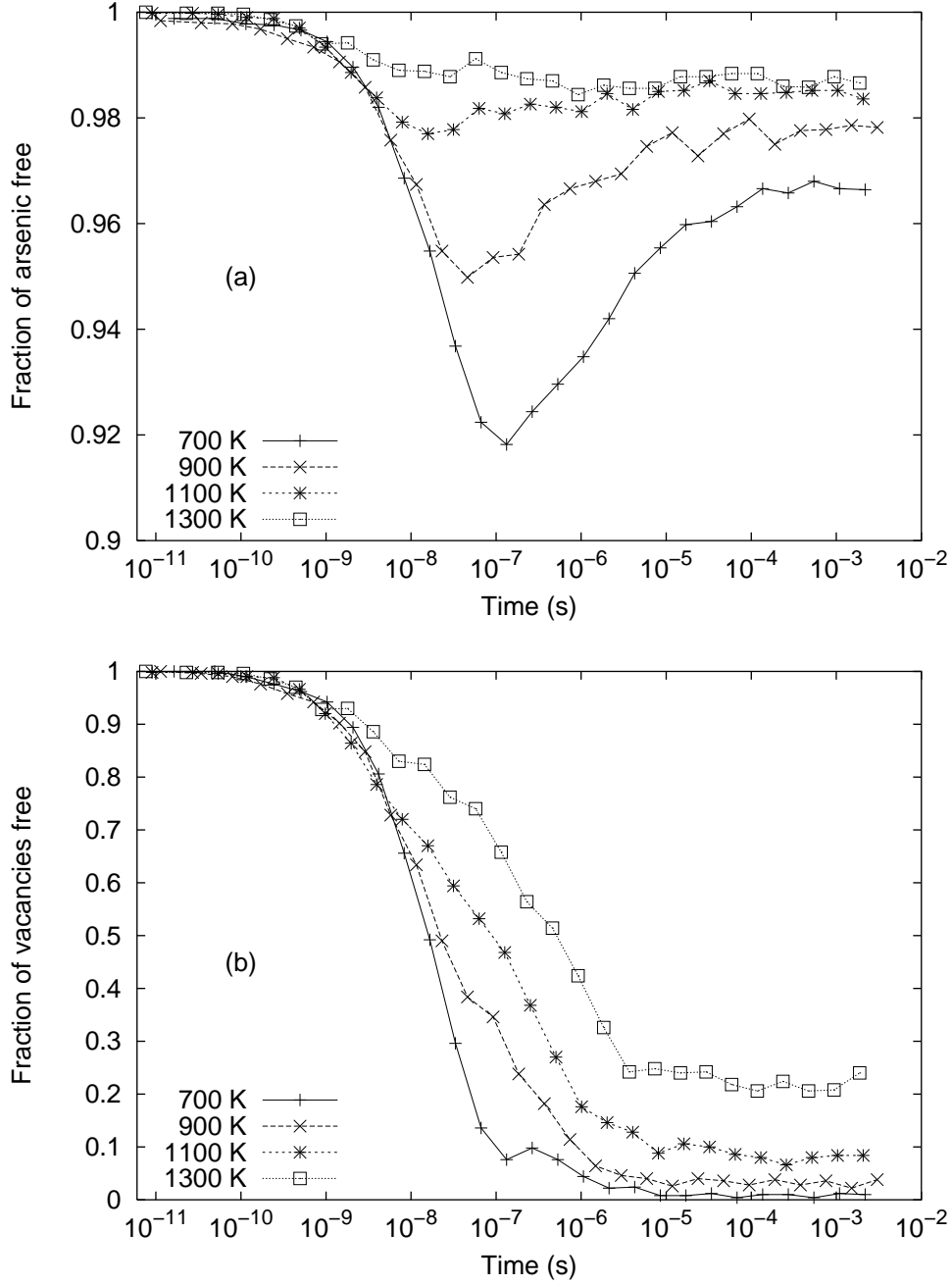


FIG. 3: Fraction of arsenic (a) and vacancies (b) free over time for various temperatures, with arsenic concentration  $10^{19} \text{ cm}^{-3}$  and vacancy concentration  $10^{18} \text{ cm}^{-3}$  and 18 shell interactions.

seconds. This result expands the work of Bunea and Dunham<sup>3</sup>, who found little deviation from the pair diffusion model at lower temperature but did not consider time dependence. It should be noted that the results of Bunea and Dunham were obtained by simulating a single arsenic-vacancy pair with interactions ranging from third to sixth nearest lattice neighbor.

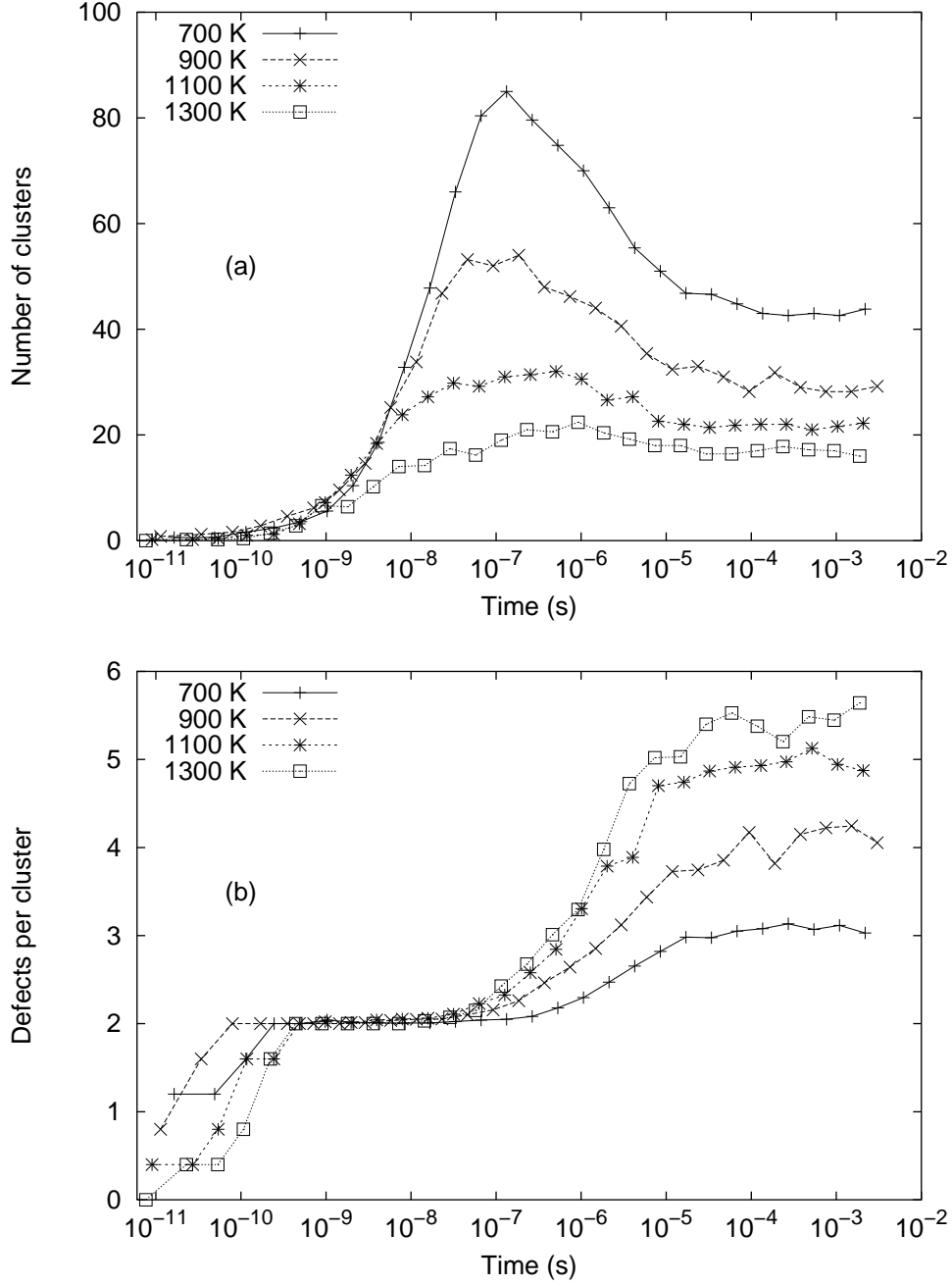


FIG. 4: Number of clusters (a) and defects per cluster (b) over time for various temperatures, with arsenic concentration  $10^{19} \text{ cm}^{-3}$  and vacancy concentration  $10^{18} \text{ cm}^{-3}$  and 18 shell interactions.

## B. Interaction range

In order to study the effect of interaction range on arsenic diffusion and clustering, we truncated and shifted the interaction potentials in Figure 1 from 18 shells to 12, 6, and 4 shells, so that the interaction vanishes at the indicated separation. The system temperature,

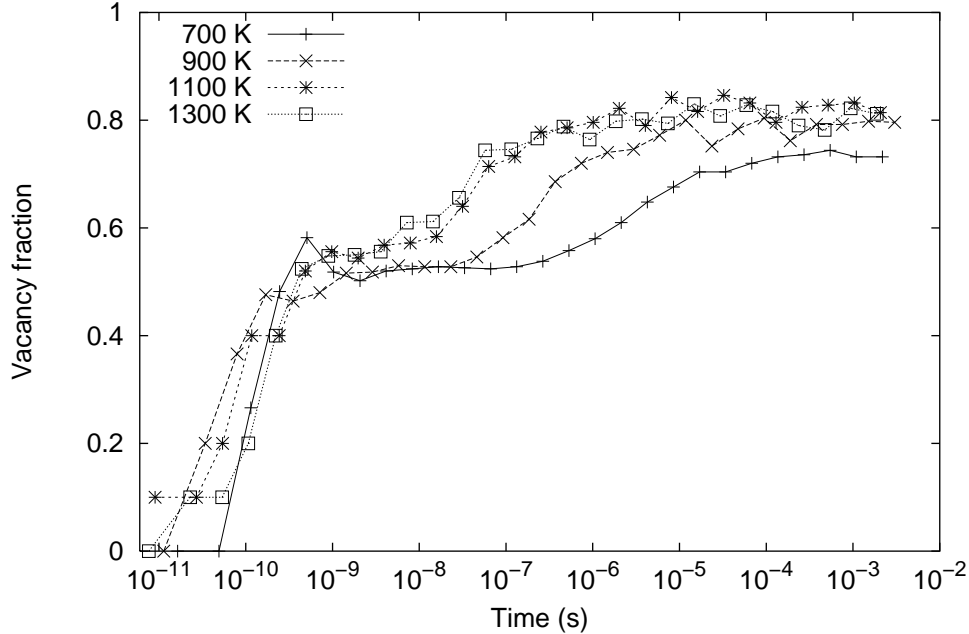


FIG. 5: Vacancy fraction of defects in clusters over time for various temperatures, with arsenic concentration  $10^{19} \text{ cm}^{-3}$  and vacancy concentration  $10^{18} \text{ cm}^{-3}$  and 18 shell interactions.

the number of arsenic and vacancies, and the system size remained constant. Figure 6 shows the diffusivity of arsenic and vacancies, again calculated using equation (5), over time for interaction ranges of 18, 12, 6, and 4 shells. Those simulations with the longest range interactions show an initial transient behavior until  $10^{-5}$  seconds, after which the diffusivity is constant over time. In contrast, for shorter interaction ranges, the diffusivity continues to decrease over time. Figure 7 shows the fraction of each species free over time. For all interaction ranges considered, the fraction of free arsenic decreases as arsenic-vacancy pairs (AsV) form, but for 4, 6, and 12 shell interactions, almost all arsenic are free from clusters at later times and thus immobile. For 18 shell interactions, the fraction of arsenic free remains roughly constant over the same time range that arsenic diffusivity is constant. For vacancies, 18 shell interactions allow some vacancies to remain free at all times, while shorter range interactions lead to a state in which all vacancies in the system are bound in clusters. Figure 8 presents the number of clusters and defects per cluster over time for the interaction ranges of interest. When considering 18 shell interactions, both quantities reach a somewhat constant level over time, while all shorter range interactions cause the number of clusters to continue to decrease and the size of the clusters to increase. Combined with the free fractions in Figure 7, this implies that AsV form initially, for times up to  $10^{-7}$  seconds, after

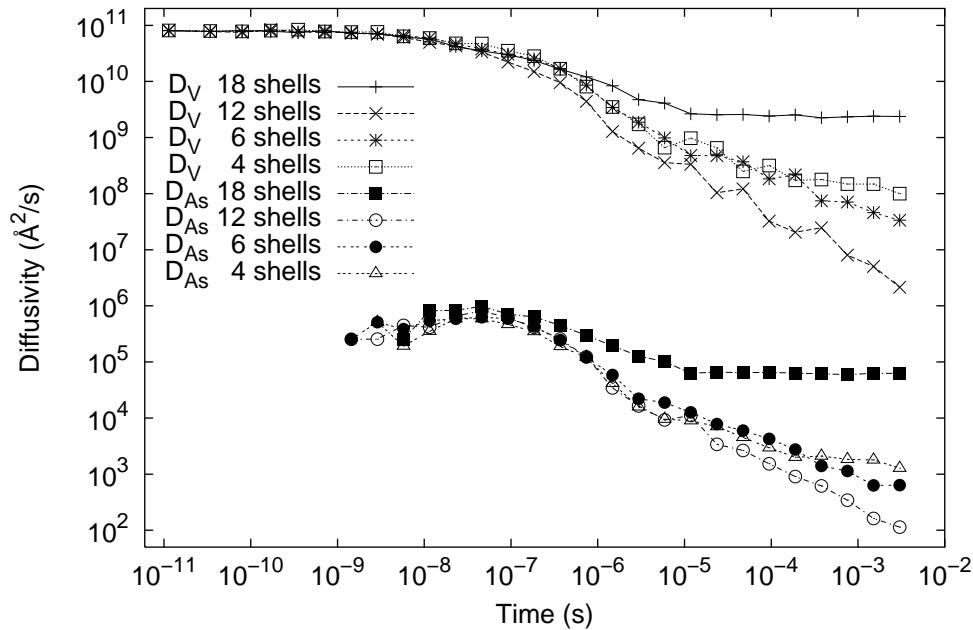


FIG. 6: Diffusivity of arsenic and vacancies over time for various interaction ranges, with arsenic concentration  $10^{19} \text{ cm}^{-3}$  and vacancy concentration  $10^{18} \text{ cm}^{-3}$  at 900 K.

which, as AsV begin to interact, the short range vacancy-vacancy interaction overwhelms all other interactions; the AsV dissociate, the arsenic atoms are left isolated and immobile, and the vacancies cluster with each other. This can be seen more clearly in Figure 9; for shorter interaction ranges, almost all defects in clusters are vacancies at long times. The strong interaction between vacancies at short range dominates the clustering behavior of the system if no longer-range interactions are included.

### C. Concentration

The concentration of dopants in the system can be varied by two methods. Either the dimensions of a simulation cell with periodic boundary conditions or the number of dopants in the cell can change. The diffusivities for both arsenic and vacancies, calculated using equation (5), are virtually identical over time for each method at high concentrations. At low concentrations, some time dependent differences emerge in diffuse systems. We chose to vary arsenic concentration by changing the size of the simulation cell, with periodic boundary conditions, maintaining a constant number of arsenic and vacancies in the system. This method is much more computationally efficient, as the simulation time increases with the

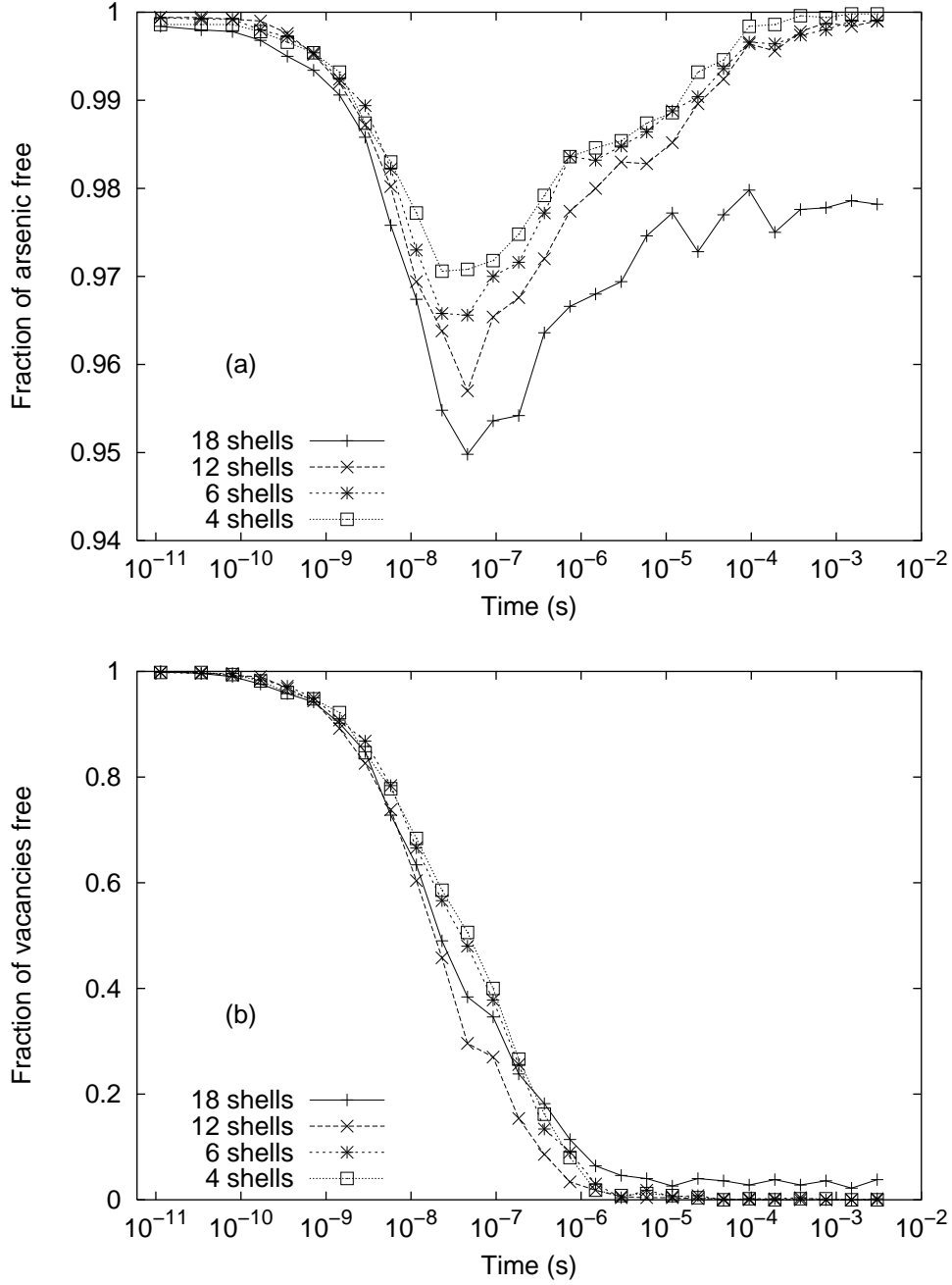


FIG. 7: Fraction of arsenic (a) and vacancies (b) free over time for various interaction ranges, with arsenic concentration  $10^{19} \text{ cm}^{-3}$  and vacancy concentration  $10^{18} \text{ cm}^{-3}$  at 900 K.

number of defects in the system. The system temperature and the interaction range are constant, as well.

Figure 10 shows the diffusivity, calculated using equation (5), of arsenic and vacancies over time for arsenic concentrations ranging from  $10^{17} \text{ cm}^{-3}$  to  $10^{21} \text{ cm}^{-3}$ . The arsenic

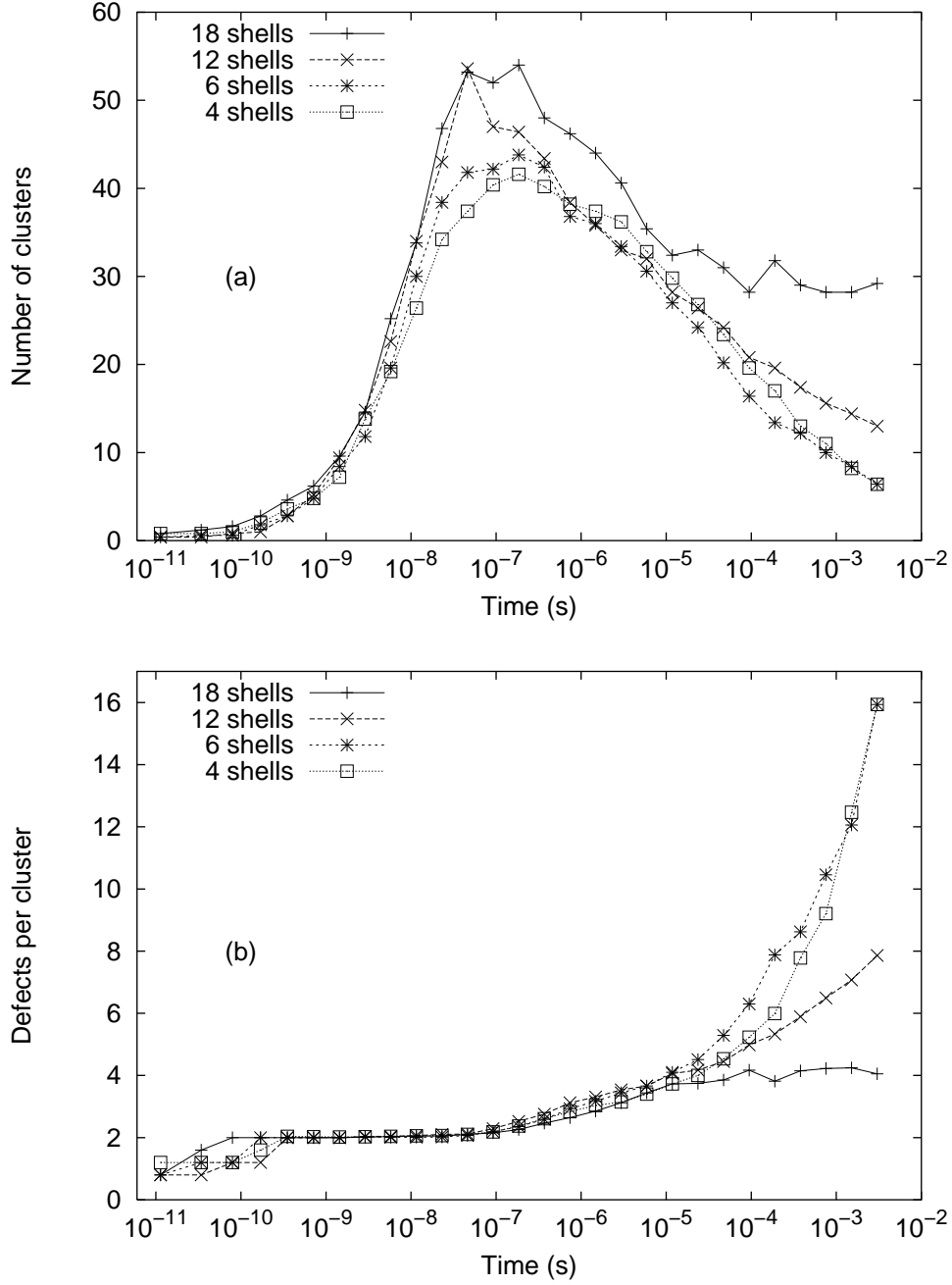


FIG. 8: Number of clusters (a) and defects per cluster (b) over time for various interaction ranges, with arsenic concentration  $10^{19} \text{ cm}^{-3}$  and vacancy concentration  $10^{18} \text{ cm}^{-3}$  at 900 K.

diffusion begins as arsenic-vacancy pairs (AsV) form, which happens earlier as the arsenic concentration increases. At the highest arsenic concentration considered,  $10^{21} \text{ cm}^{-3}$ , there is almost no free diffusion of vacancies, due to the long range interactions. Figure 10a shows that, while arsenic diffusivity is initially higher at greater arsenic concentrations, by  $10^{-5}$

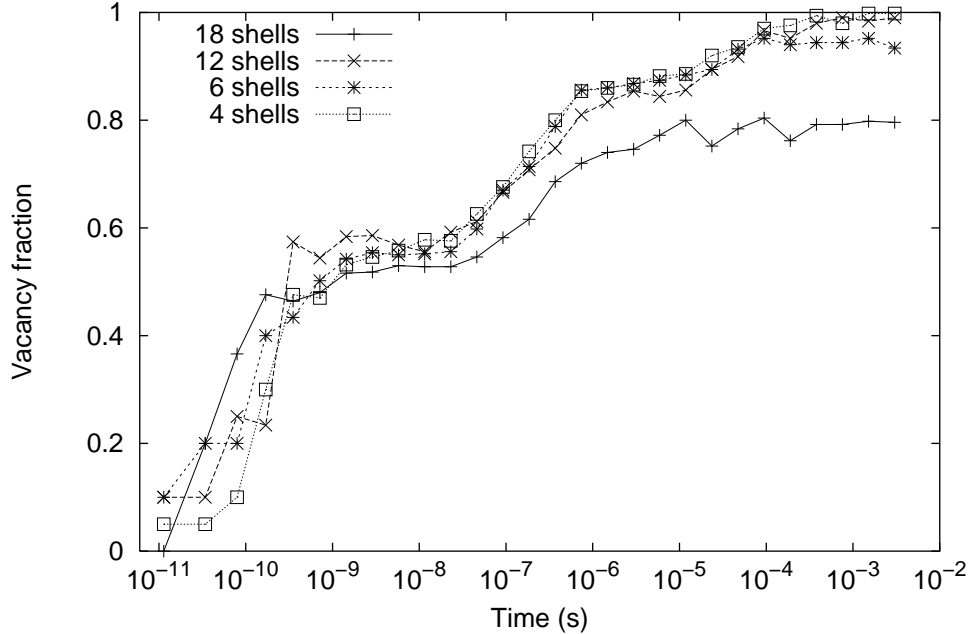


FIG. 9: Vacancy fraction of defects in clusters over time for various interaction ranges, with arsenic concentration  $10^{19} \text{ cm}^{-3}$  and vacancy concentration  $10^{18} \text{ cm}^{-3}$  at 900 K.

seconds, the maximum arsenic diffusivity occurs for concentrations in the range of  $10^{18} \text{ cm}^{-3}$  to  $10^{19} \text{ cm}^{-3}$ , while concentrations greater and less than this range yield a lower diffusivity. This is the same trend observed experimentally by Fair and Weber<sup>6</sup>, although the peak diffusivity measured in that work was at  $3 \times 10^{20} \text{ As cm}^{-3}$ , at a temperature of 1000 °C. The results in Figure 10a show a different trend than the experimental work of Larsen *et al.*<sup>7</sup> and the KLMC results of Dunham and Wu<sup>9</sup>. Both of those studies, conducted at 1050 °C, found an increase in arsenic diffusivity for dopant concentrations above  $2 \times 10^{20} \text{ cm}^{-3}$ . The simulations of Dunham and Wu considered third nearest neighbor interactions which decreased linearly with distance. Our results also disagree with those of Bunea and Dunham<sup>10</sup>, who found greater enhancement in arsenic diffusivity at higher arsenic concentrations for short simulation times at 900 °C; the effect they reported decreased over long simulation times. It should be noted that the simulations of Bunea and Dunham considered interactions ranging from the third to sixth nearest lattice neighbor, in contrast to our long range interactions.

Figure 11 shows that the number of clusters over time is greater as arsenic concentration increases, and that the typical cluster size is roughly the same for different doping levels. This alone does not explain why arsenic diffusivity is not enhanced at greater concentrations, but Figure 12 shows that as the arsenic concentration increases, the fraction of vacancies in

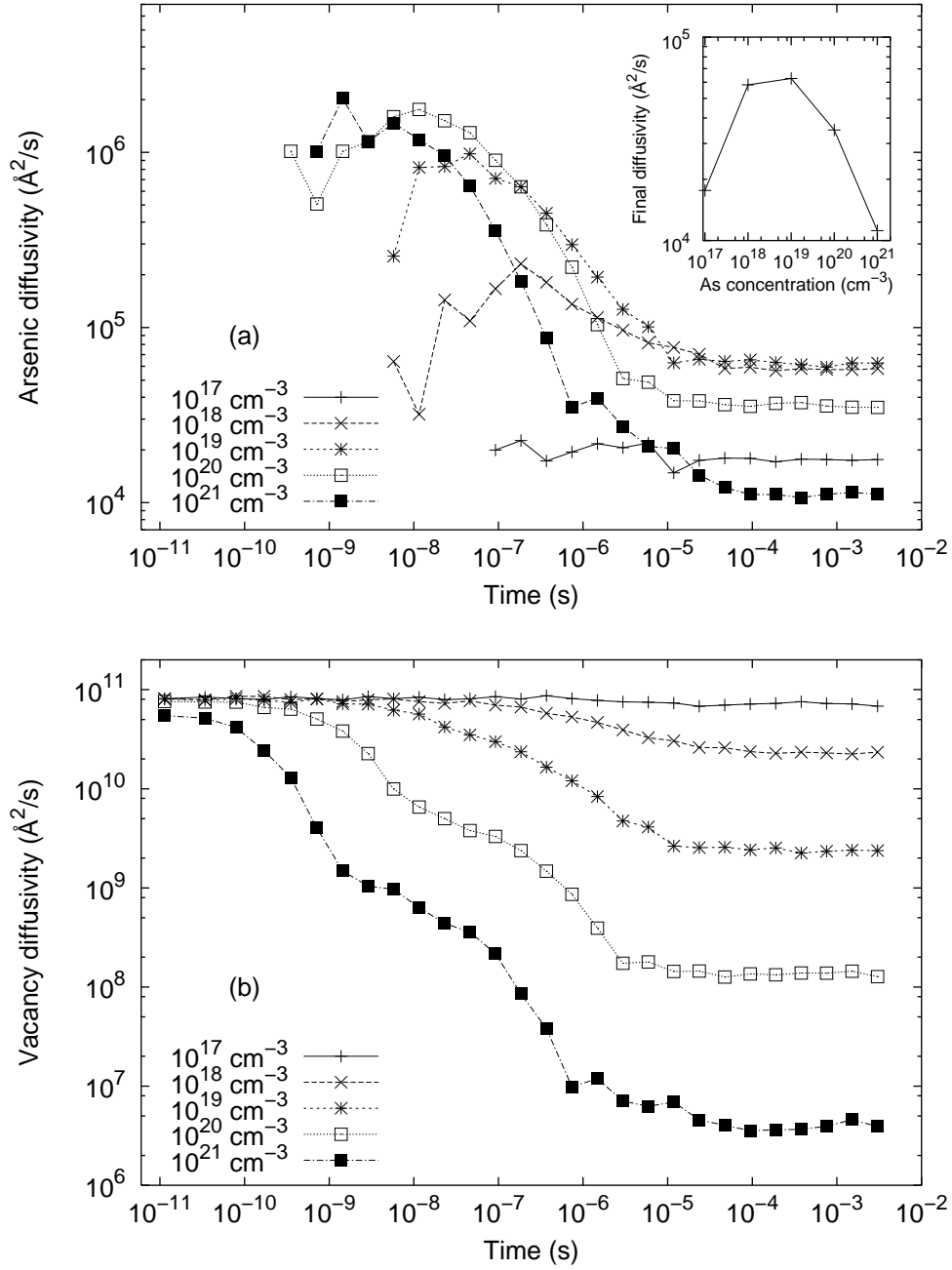


FIG. 10: Diffusivity of arsenic (a) and vacancies (b) over time for various arsenic concentrations, with arsenic:vacancy ratio of 10:1 and 18 shell interactions at 900 K.

clusters decreases. Thus, at higher doping levels the arsenic fraction of defects in clusters increases. This supports the conclusions of Xie and Chen<sup>13</sup> and Bunea and Dunham<sup>10</sup> who suggested the development of large, arsenic dominated clusters at elevated doping levels.

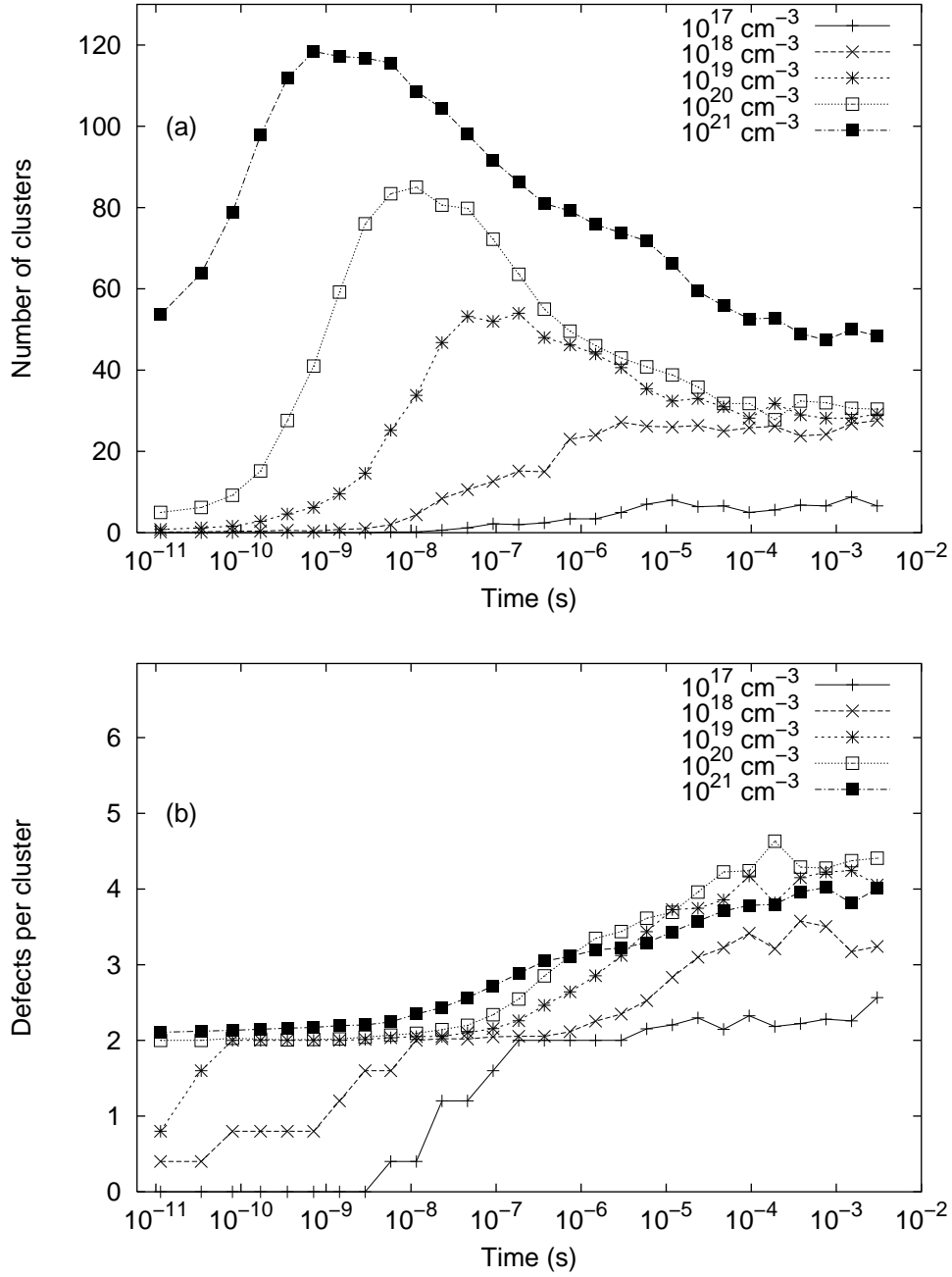


FIG. 11: Number of clusters (a) and defects per cluster (b) over time for various arsenic concentrations, with arsenic:vacancy ratio of 10:1 and 18 shell interactions at 900 K.

#### D. Defect ratio

Immediately after ion implantation, the concentration of vacancies should be much higher than the equilibrium concentration. We have assumed a baseline vacancy concentration of  $10^{18} \text{ cm}^{-3}$  in this work, for an arsenic:vacancy ratio of 10:1. In order to explore the ramifi-

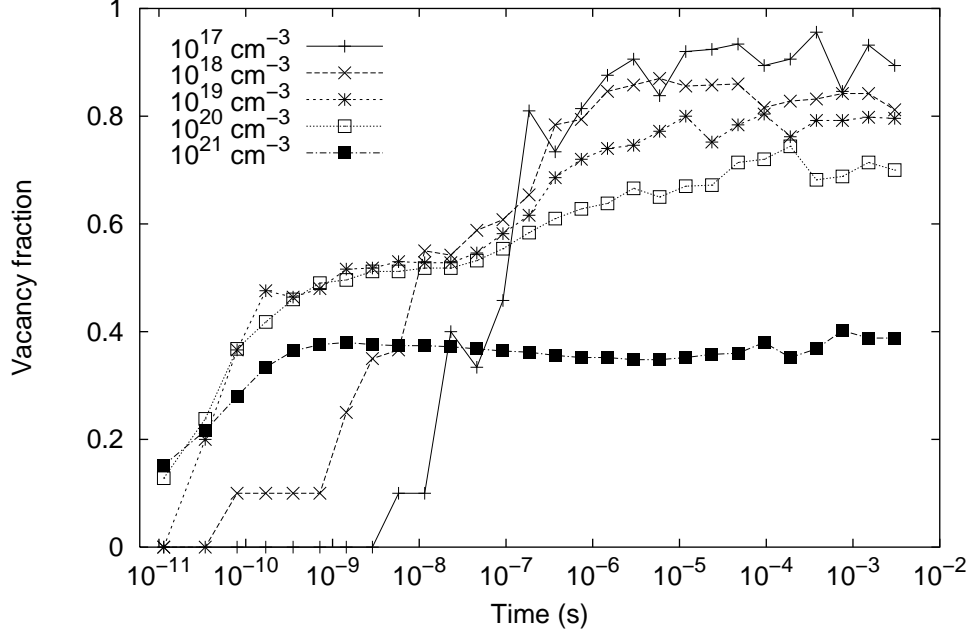


FIG. 12: Vacancy fraction of defects in clusters over time for various arsenic concentrations, with arsenic:vacancy ratio of 10:1 and 18 shell interactions at 900 K.

cations of this choice, we performed KLMC simulations at several different arsenic:vacancy ratios, ranging from 2:1 to 200:1, with a constant arsenic concentration of  $10^{19} \text{ cm}^{-3}$ . The arsenic:vacancy ratio of 200:1 corresponds to the equilibrium vacancy concentration used in previously cited KLMC works. The system temperature, the interaction range, and the size of the simulation cell were held constant. Figure 13 shows the diffusivities of arsenic and vacancies, calculated using equation (5), for various arsenic:vacancy ratios. The diffusivity of arsenic is greater with more vacancies in the system. Conversely, vacancy diffusivity is lower with more vacancies in the system. Figure 14 supports this trend. With fewer vacancies in the system, a greater fraction of both arsenic and vacancies will be free over time.

In Figure 15 we see that a greater number of vacancies produces both a higher number of clusters and larger clusters, and Figure 16 shows that the vacancy fraction of defects in clusters will increase with vacancy concentration. Thus, having more vacancies in the system leads to more clusters, larger clusters, and more vacancies in the clusters. This is most likely due to the strong vacancy-vacancy interaction at short range.

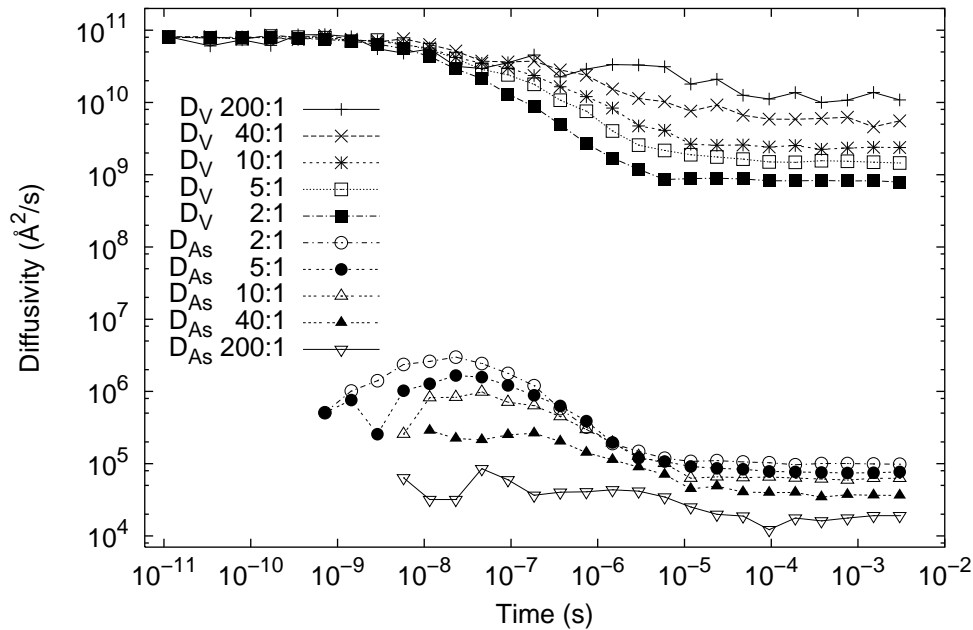


FIG. 13: Diffusivity of arsenic and vacancies over time for various arsenic:vacancy ratios, with arsenic:vacancy ratio of 10:1 and 18 shell interactions at 900 K.

#### IV. CONCLUSION

We have presented results of kinetic lattice Monte Carlo simulations using long range interactions, to the 18th nearest lattice neighbor, and large numbers of defects, including 1000 arsenic atoms and a high vacancy concentration, which would be found shortly after implantation of dopant atoms into silicon. We demonstrated that the trend at higher temperatures is toward fewer clusters with more defects. At all investigated temperatures, the vacancy fraction of defects in clusters increases over time. At low temperatures, this implies the dissociation of some arsenic-vacancy pairs (AsV), after which the newly free vacancy attaches to a nearby AsV. At higher temperatures, mobile AsV attract free vacancies. In both cases, a diffusion model based only on arsenic-vacancy pairs may be inadequate because of time dependent clustering effects.

We also demonstrated that considering only short interaction ranges, less than 18 shells, produces mostly vacancy clusters, due to the strong short range attraction between vacancies. This behavior manifests itself in decreasing diffusivities over time, exclusion of arsenic from clusters as AsV dissociate, decreasing number of clusters while cluster size grows, and vacancy fraction of defects in clusters approaching 1 over time. Such behavior implies that

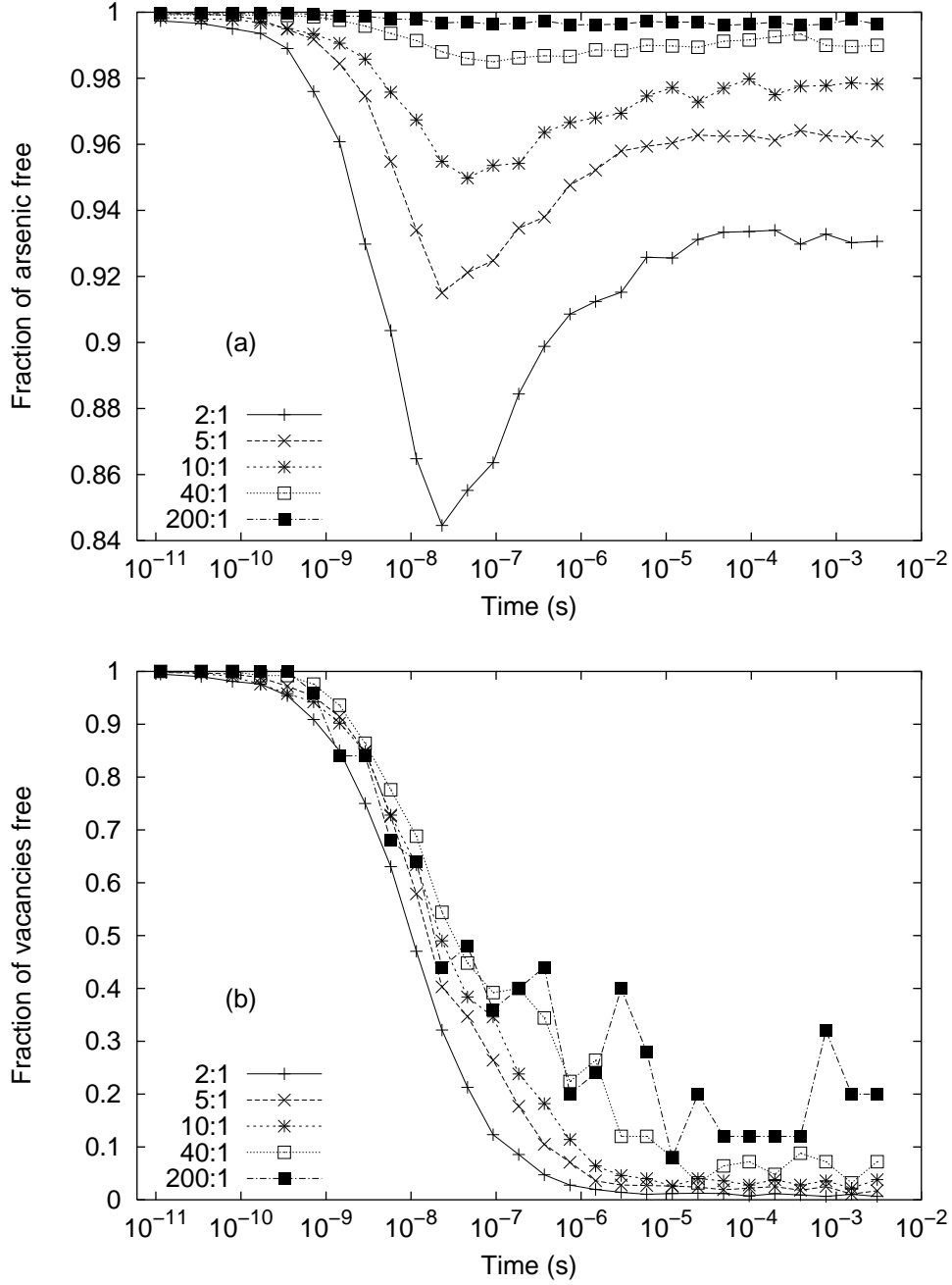


FIG. 14: Fraction of arsenic (a) and vacancies (b) free over time for various arsenic:vacancy ratios, with arsenic concentration  $10^{19} \text{ cm}^{-3}$  and 18 shell interactions at 900 K.

little or no arsenic diffusion is occurring and is in contradiction with experimental evidence. Therefore, long range interactions seem crucial for realistic simulations of defect migration in silicon.

We showed that arsenic diffusivity increases for arsenic concentrations up to  $10^{19} \text{ cm}^{-3}$  and then decreases as arsenic concentration increases. This behavior is due to the forma-

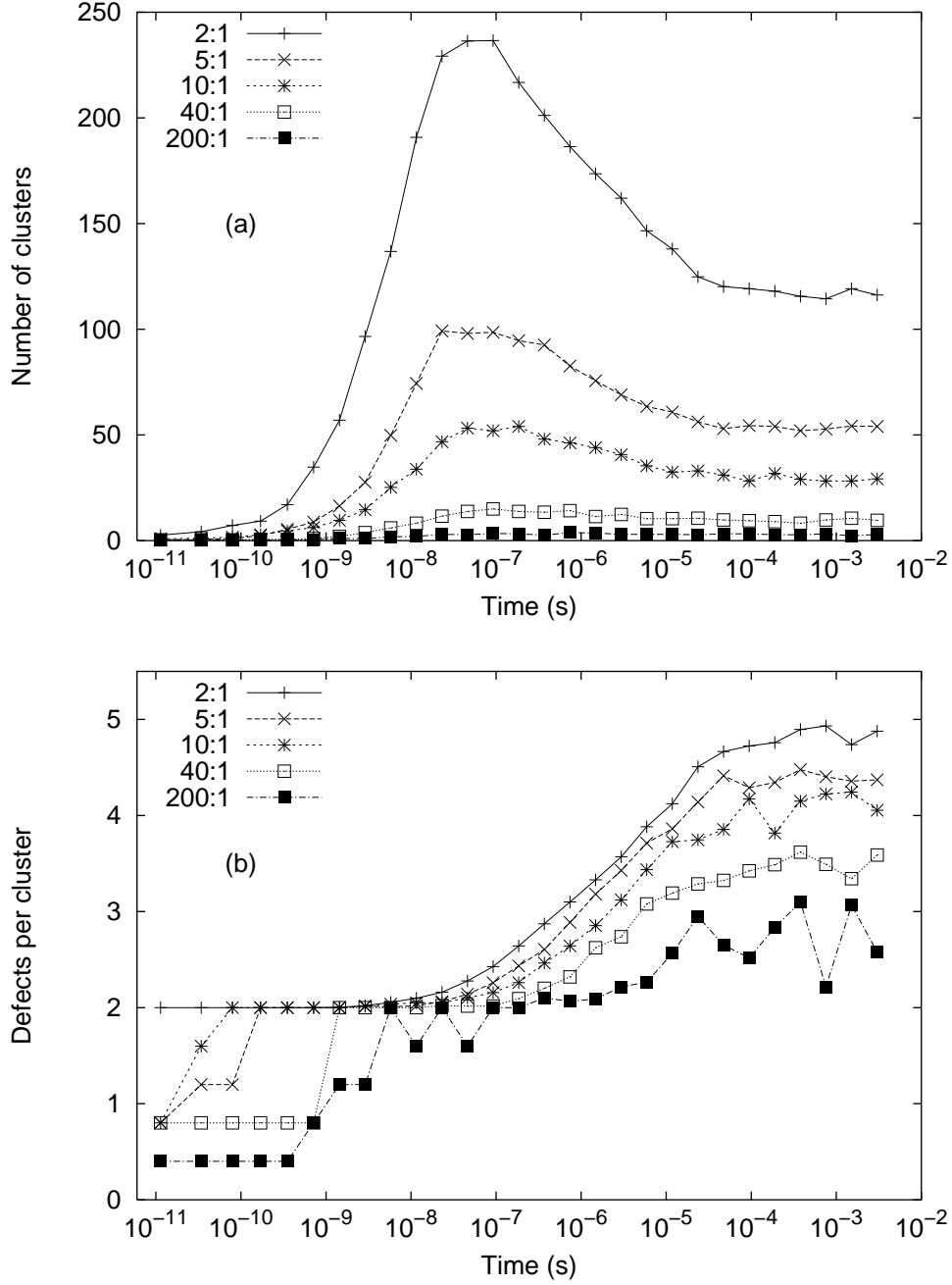


FIG. 15: Number of clusters (a) and defects per cluster (b) over time for various arsenic:vacancy ratios, with arsenic concentration  $10^{19} \text{ cm}^{-3}$  and 18 shell interactions at 900 K.

tion of a greater number of clusters at higher arsenic concentration; the size of the clusters does not increase substantially. The vacancy fraction, however, changes significantly, transitioning from vacancy dominated clusters to arsenic dominated clusters at high arsenic concentrations, keeping the arsenic:vacancy ratio constant.

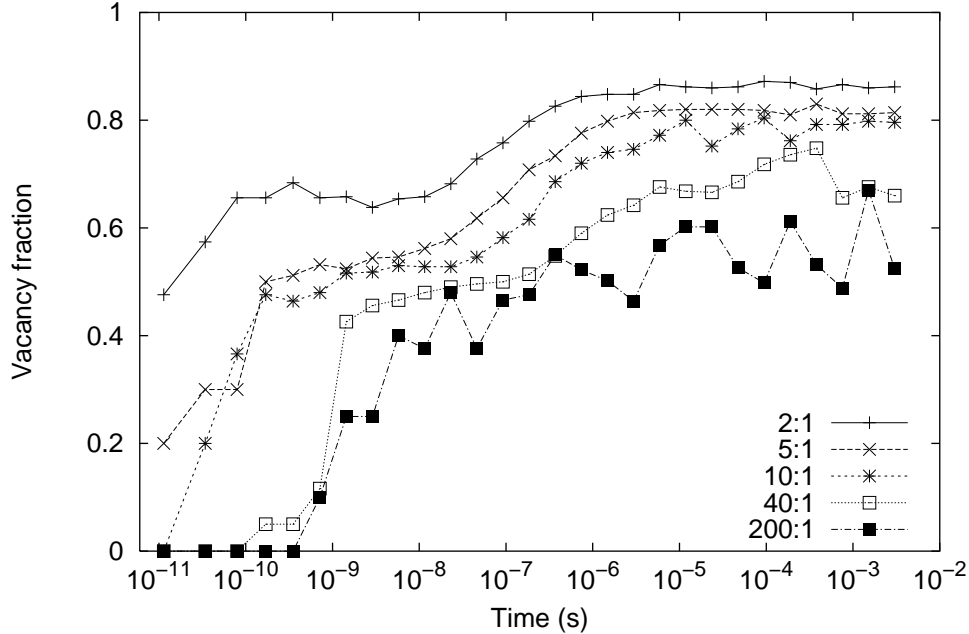


FIG. 16: Vacancy fraction of defects in clusters over time for various arsenic:vacancy ratios, with arsenic concentration  $10^{19} \text{ cm}^{-3}$  and 18 shell interactions at 900 K.

Lastly we studied diffusion and clustering behavior as a function of the number of vacancies in the system. We concluded that higher concentrations of vacancies lead to larger clusters, more clusters, and more vacancies per cluster. While a large vacancy concentration is expected immediately after ion implantation, this may not be realistic at later times. More work is needed to incorporate interstitial defects, especially silicon self interstitials so that Frenkel pair recombination can change the vacancy concentration over time.

### Acknowledgments

We thank Keith M. Beardmore for contributing the VASP interaction potentials, Lin-Wang Wang and Andrew Canning of the Lawrence Berkeley National Laboratory for the PEtot code and advice on the calculations, and Mike Masquelier and Wolfgang Windl for useful discussions in the early stages of the work. Initial part of the work was supported by the Computational Nanoscience Group of Motorola, Inc.

---

<sup>1</sup> P. M. Fahey, P. B. Griffin, and J. D. Plummer, Rev. Mod. Phys **61**, 289 (1989).

- <sup>2</sup> K. M. Beardmore, W. Windl, B. P. Haley, and N. Grønbech-Jensen, in *Proc. 2002 International Conference on Computational Nanoscience* (Computational Publications, Cambridge, MA, 2002), p. 466.
- <sup>3</sup> M. M. Bunea and S. T. Dunham, *Phys. Rev. B* **61**, 2397 (2000).
- <sup>4</sup> A. Fick, *Ann. Phys. Chem.* **94**, 59 (1855).
- <sup>5</sup> O. Pankratov, H. Huang, T. D. de la Rubia, and C. Mailhot, *Phys. Rev. B* **56**, 13172 (1997).
- <sup>6</sup> R. B. Fair and G. R. Weber, *J. Appl. Phys.* **44**, 273 (1973).
- <sup>7</sup> A. N. Larsen, K. K. Larsen, and P. E. Andersen, *J. Appl. Phys.* **73**, 691 (1993).
- <sup>8</sup> S. Solmi and D. Nobili, *J. Appl. Phys.* **83**, 2484 (1998).
- <sup>9</sup> S. T. Dunham and C. D. Wu, *J. Appl. Phys.* **78**, 2362 (1996).
- <sup>10</sup> M. M. Bunea and S. T. Dunham, in *Defects and Diffusion in Silicon Processing* (Mat. Res. Soc., 1997), vol. 469, p. 353.
- <sup>11</sup> S. List and H. Ryssel, *J. Appl. Phys.* **83**, 7595 (1998).
- <sup>12</sup> H. Bracht, N. A. Stolwijk, I. Yonenaga, and H. Meherer, *Phys. Stat. Sol.* **137**, 499 (1994).
- <sup>13</sup> J. Xie and S. P. Chen, *Phys. Rev. Lett.* **83**, 1795 (1999).
- <sup>14</sup> A. Ural, P. B. Griffin, and J. D. Plummer, *J. Appl. Phys.* **85**, 6440 (1999).
- <sup>15</sup> M. Tang, L. Colombo, J. Zhu, and T. D. de la Rubia, *Phys. Rev. B* **55**, 14279 (1997).
- <sup>16</sup> K. M. Beardmore, private communication.
- <sup>17</sup> G. Kresse and J. Furthmüller, *Phys. Rev. B* **54**, 11169 (1996).
- <sup>18</sup> H. J. Monkhorst and J. D. Pack, *Phys. Rev. B* **13**, 5188 (1976).
- <sup>19</sup> URL <http://crd.lbl.gov/~linwang/PEtot/PEtot.html>.